Balanitin-6 and -7: Diosgenyl saponins isolated from *Balanites aegyptiaca* Del. display significant anti-tumor activity *in vitro* and *in vivo*

CHARLEMAGNE GNOULA[1,2], VÉRONIQUE MÉGALIZZI[3], NANCY DE NÈVE[4], SÉBASTIEN SAUVAGE[4], FABRICE RIBAUCOUR[4], PIERRE GUISSOU[5], PIERRE DUEZ[2], JACQUES DUBOIS[1], LAURENT INGRASSIA[4], FLORENCE LEFRANC[3,6], ROBERT KISS[3] and TATJANA MIJATOVIC[4]

[1]Laboratoire de Chimie Bioanalytique, de Toxicologie et de Chimie Physique Appliquée, Institut de Pharmacie, [2]Laboratoire de Pharmacognosie, de Bromatologie et de Nutrition Humaine, [3]Laboratoire de Toxicologie, Institut de Pharmacie, Université Libre de Bruxelles (ULB); [4]Unibioscreen SA, Brussels, Belgium; [5]Laboratoire de Pharmacologie, Faculté des Sciences de la Santé, Université de Ouagadougou, Ouagadougou, Burkina Faso; [6]Département de Neurochirurgie, Cliniques Universitaires de Bruxelles, Hôpital Erasme, ULB, Brussels, Belgium

Received July 24, 2007; Accepted September 10, 2007

Abstract. *Balanites aegyptiaca* is a widely distributed African plant of medicinal interest containing a number of cytotoxic and cytostatic compounds. The studies reported here have attempted to further characterize the anti-cancer activity of a mixture of steroidal saponins: balanitin-6 (28%) and balanitin-7 (72%) isolated from *Balanites aegyptiaca* kernels. The balanitin-6 and -7 mixture (henceforth referred to as bal6/7) has demonstrated appreciable anti-cancer effects in human cancer cell lines *in vitro*. Bal6/7 displayed higher anti-proliferative activity than etoposide and oxaliplatin, although the mixture was appreciably less active than SN38 and markedly less active than taxol. Bal6/7 demonstrated highest activity against A549 non-small cell lung cancer (NSCLC) (IC_{50}, 0.3 μM) and U373 glioblastoma (IC_{50}, 0.5 μM) cell lines. The current study has further indicated that bal6/7 is more a cytotoxic compound than a cytostatic one. However, Bal6/7 does not appear to mediate its anti-proliferative effects by inducing apoptotic cell death. Computer-assisted cellular imaging has revealed that bal6/7 does not induce detergent-like effects in A549 NSCLC and U373 glioblastoma unlike certain saponins. Furthermore there is indication that its *in vitro* anti-cancer activities result at least partly from depletion of $[ATP]_i$, leading in turn to major disorganization of actin cytoskeleton, ultimately resulting in the impairment of cancer cell proliferation and migration. In contrast to a number of natural products acting as anti-cancer agents, bal6/7 does not induce an increase in intra-cellular reactive oxygen species. *In vivo*, bal6/7 increased the survival time of mice bearing murine L1210 leukemia grafts to the same extent reported for vincristine. These preliminary *in vivo* data suggest that it may be possible to generate novel hemi-synthetic derivatives of balanitin-6 and -7 with potentially improved *in vitro* and *in vivo* anti-cancer activity and reduced *in vivo* toxicity, thus markedly improving the therapeutic ratio.

Correspondence to: Dr Robert Kiss, Laboratory of Toxicology, Institute of Pharmacy, Free University of Brussels (ULB), Campus de la Plaine, Boulevard du Triomphe, CP205/01, 1050 Brussels, Belgium
E-mail: rkiss@ulb.ac.be

Key words: balanitin, diosgenyl saponins

Introduction

Balanites aegyptiaca Del. (Balanitaceae) is a widely distributed African plant of medicinal interest (1,2). It is a small spinescent evergreen savanna tree with a dark brown stem which usually attains a height of 4.5-6 m (3). In Egyptian folk medicine, the fruits are used as an oral hypoglycemic (4) and an anti-diabetic (5). An aqueous extract of the fruit mesocarp is used in Sudanese folk medicine in the treatment of jaundice (5) and as an anthelmintic (3). Indeed the plant is used as a purge to remove intestinal parasites with the root, branches, bark, fruit and kernel extracts shown to be lethal to the miracidia and cercariae of *Shistosoma mansoni* and to *Fasciola gigantica* (3,6). Additionally extracts of the tree display abortive and antiseptic properties (2).

The bark of *Balanites aegyptiaca* contains a number of alkaloids such as N-trans-feruloyltyramine and N-cis-feruloyltyramine (5) and common phenolic compounds such as vanillic acid, syringic acid and 3-hydroxy-1-(4-hydroxy-3-methoxyphenyl)-1-propanone (5). The roots and bark also contain numerous steroidal saponins and yamogenin or diosgenin glycosides (2). The fruit mesocarp contains a large variety of chemicals amongst which are the pregnane glycosides (1), coumarins (2), flavonoids (2), 6-methyl-diosgenin (2) and furostanol saponins (1,4). The saponins are a structurally and biologically diverse class of glycosides of both steroids and triterpenes that are widely distributed in terrestrial plants and in some marine organisms (7). Diosgenyl

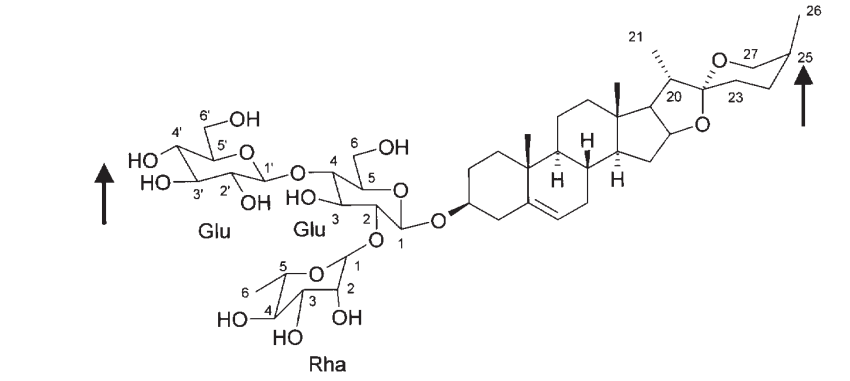

Balanitin-6

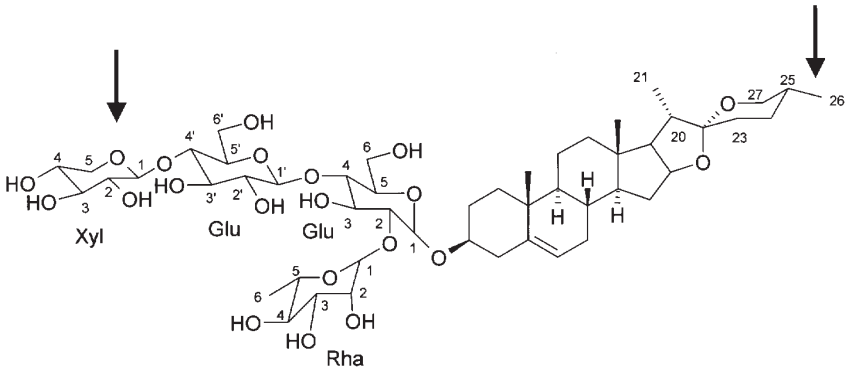

Balanitin-7

Figure 1. Chemical structures of balanitin-6 and -7. The arrows point to the differences between balanitin-6 and balanitin-7: the lack of a xylose in balanitin-6 when compared to balanitin-7 and an axial C26 methyl position for balanitin-6 (yamogenin) and an equatorial for balanitin-7 (diosgenin).

saponins are the most abundant (7) and present typical oligosaccharide chains in which the first sugar, ß-D-glucopyranoside is attached to diosgenin via the 3-OH position, and the ß-D-glucopyranoside is itself substituted via its 2-OH and 4-OH positions respectively by α-L-rhamnopyranose and other sugars or sugar chains. Dioscin, polyphyllin D and balanitins (Fig. 1) belong to this class (7).

Methanol and butanol extracts of *Balanites aegyptiaca* initially afforded two novel saponins with anti-inflammatory properties, balanitin-1 and -2 (2). Bioactivity-guided separation of a CH_2Cl_2/MeOH extract of *Balanites aegyptica* identified four further novel balanitins, -4, -5, -6 and -7, which were found to have cytostatic activity (Fig. 1) (8).

The aim of the present study was to further characterize the anti-tumor activity of balanitin-6 and -7 and to decipher their mechanism(s) of action. For this purpose, a mixture containing balanitin-6 and -7 (bal6/7: ~28% and 72%, respectively) extracted from *Balanites aegyptiaca* kernels was evaluated *in vitro* for anti-cancer activity against six different human cancer cell lines using the MTT colorimetric assay (9) and *in vivo* in the murine L1210 leukemia model (16). Additionally, computer-assisted quantitative videomicroscopy (10-13) has been used to investigate how bal6/7 reduces the overall growth rate of A549 non-small cell lung cancer [NSCLC; (14)] and U373 glioblastoma (15) cell lines, and whether bal6/7 destroys cancer cells simply by detergent-related effects. Additionally the impact of bal6/7 on intra-cellular concentrations of ATP $[ATP]_i$ and reactive oxygen species $[ROS]_i$ and the organization of the actin cytoskeleton have been investigated.

Materials and methods

Balanitin isolation. Balanitin-6 and -7 have been isolated from *Balanites aegyptiaca* using a procedure similar to one previously described (8). Powdered kernels (504 g) from *Balanites aegyptiaca* were extracted with distilled water (4 times with 1.5 l) over 3 h at ambient temperature and the combined extracts filtered and reduced in volume to obtain a concentrate (500 ml). The concentrate was then extracted with an equal volume of *n*-butanol which on evaporation yielded 39 g of solid matter. This solid was dissolved in methanol (125 ml) and then chromatographed on an LH-20 column (2.5 kg; 105x10 cm) using methanol (25 l) as the eluent. Eluted fractions were monitored by TLC using CH_2Cl_2/MeOH (v/v: 8/2) as the solvent. All fractions containing a component with an Rf of 0.27 were combined and evaporated

A

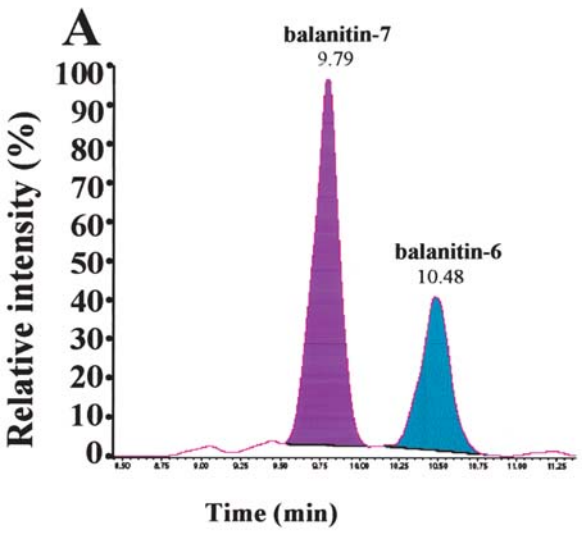

C

m/z	fragments	% Relative intensity
1039	$[M+Na]^+$	2.6
1017	$[M+H]^+$	1.1
885	$[M+H-132]^+$	0.5
871	$[M+H-146]^+$	0.4
739	$[M+H-278]^+$	2.6
723	$[M+H-294]^+$	11.7
577	$[M+H-440]^+$	18.1
415	$[M+H-602]^+$	55.1
271	$[M+H-746]^+$	100

B

carbon	Bal-6	Bal-7	Our sample
23	26.40	31.86	30.16 26.42
24	26.21	29.30	29.31 26.24
25	27.54	30.63	30.65 27.58
C-1 Xylose	-	106.36	106.31
C-1' Glucose	105.23	104.61	105.21 104.57
C-1 Glucose	101.79	101.80	101.80
C-1 Rhamnose	100.00	99.98	99.95

D

m/z	fragments	% Relative intensity
907	$[M+Na]^+$	6.6
885	$[M+H]^+$	7.3
739	$[M+H-146]^+$	3.9
723	$[M+H-162]^+$	7.1
577	$[M+H-308]^+$	15
415	$[M+H-470]^+$	58.5
271	$[M+H-614]^+$	100

Figure 2. Chromatographic separation of balanitin-6 and -7 and confirmation of structures. A, LC-MS total ion current (TIC) chromatogram of the final isolated mixture of balanitin-6 (Rt, 10.48 min) and balanitin-7 (Rt, 9.79 min). The LC-MS TIC chromatograph of the sample was obtained by monitoring for a characteristic fragment ion at m/z 271 common to both balanitin-6 and -7. The units of the x-axis are retention time expressed in minutes, while the units of the y-axis are the relative abundance of each compound expressed as a percentage. The relative abundance should be considered an estimate given that TIC determinations have to make the assumption of an identical level of ionization/fragmentation for balanitin-6 and -7, which may not be the case. B, ^{13}C-NMR: characteristic chemical shifts (δ ppm) for balanitin-6 and -7 from the literature in pyridine-d5 (8) and the plant isolated sample (mixture of balanitin-6 and -7). C, ESI-MS fragment ion data for balanitin-7. The assignments of ions are given in brackets and the relative intensities expressed as percentages. The mass units which are lost correspond to the following fragments: 132, xylose; 146, rhamnose; 278, xylose + rhamnose; 294, xylose + glucose; 440, xylose + rhamnose + glucose; 602, xylose + rhamnose + two glucose moieties; and 746, fragmentation of the steroidal moiety. D, ESI-MS fragment ion data for balanitin-6. The assignments of ions are given in brackets and the relative intensities expressed as percentages. The mass units which are lost correspond to the following fragments: 146, rhamnose; 162, glucose; 308, rhamnose + glucose; 470, rhamnose + two glucose moieties; and 614, fragmentation of the steroidal moiety.

to dryness to give a solid of 24 g. This solid was redissolved in 75 ml of CH_2Cl_2/MeOH (v/v: 2/3) and re-chromatographed on a Sephadex LH-20 column with CH_2Cl_2/MeOH (v/v: 2/3) used as the eluent. Eluted fractions were again analyzed by TLC as indicated above and those containing the component of Rf of 0.27 were combined and evaporated to dryness to give 19 g of solid. This latter product was subject to flash chromatography on a silica gel column and eluted with $CHCl_3$/MeOH (v/v: 9/1) to give two fractions (0.186 g and 1.9 g after evaporation). The first fraction (containing 0.186 g of the product with a TLC Rf of 0.27) was subject to further flash chromatography on a C18 reverse phase column (50x3 cm) and eluted with MeOH/H_2O (v/v: 9/1) to afford a fraction containing 37 mg of a mixture of balanitin-6 and -7 (TLC Rf of 0.27 using the conditions described above).

The structures of balanitin-6 and -7 were confirmed using ESI mass spectrometry on a Micromass ZQ and ^{1}H and ^{13}C NMR spectroscopy using a Varian unity 300 instrument and by comparison with literature data (8; Fig. 2). HPLC analyses were performed on an Alliance HPLC system.

Table I. IC_{50} and IC_{75} (μM) values for *in vitro* growth inhibition of cancer cells by bal6/7 and anti-cancer cytotoxic drugs, oxaliplatin (OXA), etoposide (VP16), SN38 and taxol.

Cell lines	Compounds									
	Bal6/7		OXA		VP16		SN38		Taxol	
	IC_{50}	IC_{75}	IC_{50}	IC_{75}	IC_{50}	IC_{75}	IC_{50}	IC_{75}	IC_{50}	IC_{75}
A549 (NSCLC)	0.3	0.5	3.9	>10	3.1	>10	0.04	0.5	0.009	0.2
U373 (GBM)	0.5	0.8	3.3	>10	1.4	10	0.001	0.2	0.001	0.5
PC-3 (prostate cancer)	0.9	2.4	9.2	>10	>10.0	>10	0.2	2.3	0.002	3.0
Bx-PC3 (pancreas cancer)	1.2	3.4	>10.0	>10	>10.0	>10	0.07	>10.0	0.003	>10.0
LoVo (colon cancer)	1.5	3.4	4.7	>10	4.9	>10	0.4	>10.0	0.005	>10.0
MCF-7 (breast cancer)	2.6	4.0	8.9	>10	>10.0	>10	0.03	0.3	0.001	>10.0
Mean	1.2	2.4	>6.7	>10	>6.6	>10	0.2	>3.9	0.004	>5.6

IC_{50} and IC_{75} values correspond respectively to concentrations that reduced by 50% and 75% the global growth of the cancer cell lines after three days of culturing in the presence of the compounds and are reported as the means calculated from six separate determinations. For the sake of clarity, rounded values are given (i.e. A549 NSCLC IC_{75}: 0.5 μM instead of 470 nM) and the SEM values are not reported. Additionally, it should be noted that the highest SEM value calculated was <5% of its mean value.

Compounds. Drugs were obtained as follows: taxol (Paclitaxel; S.A. Bristol-Myers Squibb, Brussels, Belgium), SN38 (7-ethyl-10-hydroxycamptothecin; Aventis, Brussels, Belgium), oxaliplatin (Inter-Chemical Ltd, ShenZhen, P.R. China), etoposide (VP16, Bristol-Myers Squibb, Brussels, Belgium) and doxorubicin (Adriamycin, Pfizer Pharmacia, Puurs, Belgium). Glycine, L-fructose and D-glucose were purchased from Sigma (Bornem, Belgium).

Culture media and cancer cell lines. All human cancer cell lines used in this study were obtained from the American Type Culture Collection (Manassas, USA) and included A549 NSCLC (ATCC code CCL-185), U373 glioblastoma (ATCC code HTB-17), PC-3 refractory prostate cancer (ATCC code CRL-1435), Bx-PC3 pancreatic cancer (ATCC code CRL-1687), LoVo colon cancer (ATCC code CCL-229) and MCF-7 breast cancer (ATCC code HTB-22) cell lines. The cells were maintained as described previously (9,13). All culture media were supplemented with a mixture of 0.6 mg/ml glutamine (GibcoBRL, Invitrogen, Merelbeke, Belgium), 200 IU/ml penicillin (GibcoBRL), 200 IU/ml streptomycin (GibcoBRL) and 0.1 mg/ml gentamycin (GibcoBRL). The FCS (GibcoBRL) was heat-inactivated for 1 h at 56˚C. The cells were incubated at 37˚C in sealed (air-tight) Falcon plastic dishes (Nunc, Invitrogen SA, Merelbeke, Belgium) in a 5% CO_2 atmosphere.

MTT colorimetric assay for global cell growth determination. Overall cell growth was assessed by means of the colorimetric MTT [3-(4,5-dimethylthiazol-2yl)-diphenyltetrazolium bromide; Sigma] assay, as detailed previously (10,13-15). The 6 cell lines were incubated for 24 h in 96-microwell plates (at a level of 10,000-40,000 cells/ml of culture medium depending on the cell type) to ensure adequate plating prior to cell growth determination. This assay of cell population growth is based on the capability of living cells to reduce the yellow product MTT to its blue metabolite formazan by reduction in mitochondria. The number of living cells after 72-h incubation in the presence or absence (control) of test compounds or reference drugs is directly proportional to the intensity of the blue, which is quantitatively measured by spectrophotometry using a DIAS microplate reader (Dynatech Laboratories) at a wavelength of 570 nm (with a reference of 630 nm). Each experiment was carried out in sextuplicate. Nine concentrations ranging from 10^{-5} to 10^{-9} M (with semi-log increases in concentration) were assayed for each tested compound under study.

Cellular imaging for visualizing bal6/7-induced effects on living cancer cells. Human A549 NSCLC and U373 glioblastoma cell migration and proliferation with and without compound treatment were visualized *in vitro* by quantitative videomicroscopy, as previously described (11-13,17).

Immunofluorescence analyses of actin cytoskeleton. For immunofluorescence analyses, cells were rinsed twice in cold PBS, fixed in 4% formol for 20 min at 4˚C and then rinsed twice more in cold PBS. Phallacidin conjugated with Alexa Fluor® 488 fluorochrome (Molecular Probes Inc., Eugene, USA) was used to label the fibrillar actin, and Alexa Fluor® 594-conjugated DNAseI (Molecular Probes Inc) to stain the globular actin. Cells were cultured for up to 6 h in the presence or absence of bal6/7 at the IC_{75} concentration (470 nM for A549 and 830 nM for U373 cells) on glass coverslips prior to staining. Fluorescence was visualized by a computer-assisted Olympus AX70 microscope (Omnilabo, Antwerp, Belgium) equipped with a Megaview2 digital camera and analySIS® software (Soft Imaging System, Munster, Germany), as detailed elsewhere (13).

Flow cytometry analyses for cell cycle and cell death determination

Cell cycle. The cell cycle kinetics of the A549 cells either treated with bal6/7 or left untreated were determined by flow

cytometry analysis of propidium iodide (PI) nuclear staining using a previously detailed methodology (18).

Apoptosis. Flow cytometry analysis of apoptotic versus non-apoptotic-related cell death was performed according to the experimental protocol detailed by Darzynkiewicz *et al* (19). Briefly, after various treatments with bal6/7 the cells were incubated in the dark in an annexin V-FITC (V) and PI solution for 15 min at 4˚C (APO-AF kit; Sigma). Data from approximately 10,000 cells were recorded for each sample. An 'XL System II' Beckman Coulter (Miami, FL) was used to give a precise definition of both the percentage of cells in the apoptotic and/or non-apoptotic compartments and the percentage of normal cells, i.e. those apparently left unaffected by the bal6/7 treatment. The so-called normal cells were negative for both the annexin V and the PI staining, while the early apoptotic cells were positive for annexin V but negative for PI. The late-apoptotic cells (whose cell membranes are perforated) were positive for both PI and annexin V. Each experiment was carried out in triplicate. Human MCF-7 breast cancer cells untreated or treated with doxorubicin (5 μM for 36 h) were used as the positive control for the experiment.

Cellular ATP measurements. $[ATP]_i$ was measured using a bioluminescence assay according to the manufacturer's instructions (Invitrogen, Merelbeke, Belgium) in A549 NSCLC and in U373 glioblastoma cells cultured in the presence or absence of bal6/7 at IC_{75} concentrations (470 and 830 nM, respectively) for 24-72 h (17). Three replicate determinations per time point were performed for each cell line.

Flow cytometry analyses for the determination of ROS production. Reactive oxygen species (ROS) production was determined using 2',7'-dichlorodihydrofluorescein diacetate (DCFH-DA; Fluka-Sigma, Bornem, Belgium). After A549 and U373 cells were treated with bal6/7 IC_{75} concentrations (470 and 830 nM, respectively) for 24-72 h, they were loaded for 1 h with DCFH-DA (20 μM) in RPMI-1640 medium without phenol-red. The acetoxymethyl group on DCFH-DA is cleaved by non-specific esterases within the cell, resulting in a non-fluorescent charged molecule that does not cross the cell membrane. Intra-cellular ROS irreversibly oxidizes the DCFH-DA to dichlorofluorescein (DCF), which is a fluorescent product. Ten thousand individual data points were collected for each sample using a Becton Dickinson FACScan flow cytometer (excitation 488 nm/emission 535 nm). Each experimental condition was evaluated in triplicate. Human MCF-7 breast cancer cells untreated or treated with H_2O_2 (4 mM for 1h) were used as the positive control for the experiment.

In vivo L1210 leukemia-related experiments. The anti-tumor activity of bal6/7 was evaluated *in vivo* in a previously described primary screening model of L1210 syngeneic murine leukemia (16). L1210 leukemia cells (10^6) were injected into 5- to 6-week old female B6D2F1 (C57BlxDBA/2f/F1) mice (Charles River, L'Arbresle, France) on day 0. Bal6/7 was then administered i.p. at dose levels of 1.25, 2.5 and 5 mg/kg from days 1 to 4 and from days 8 to 11 (regimen: 4 injections per week for 2 weeks) and the median survival time of drug-treated (T) groups was compared to that of the control (C) group which received no drug treatment to obtain the %T/C index. Each experimental group was composed of 9 mice. Animals were housed in plastic cages in light- (12 h night/day cycle), temperature- (22±2˚C) and humidity- (55±5%) controlled rooms. Rodent diet (AO4, UAR, Villemoisson, France) and water were provided *ad libitum*. All *in vivo* experiments were performed on the basis of authorization received from the Belgian Animal Ethics Committee of the Federal Department of Health, Nutritional Safety and the Environment (no. LA1230509).

Statistical analyses. Statistical analyses were performed using Statistica software (Statsoft, Tulsa, USA). Statistical comparison of control and treated groups was initially undertaken with the Kruskal-Wallis test (a non-parametric one-way analysis of variance). The levels of statistical significance associated with the %T/C survival indices were determined using Gehan's generalized Wilcoxon test.

Results

Bal6/7 IC_{50} and IC_{75} values for the inhibition of the proliferation of six human cancer cell lines. The IC_{50} and IC_{75} values determined for bal6/7 and four marketed cytotoxic drugs used to combat various types of cancers, oxaliplatin (OXA), etoposide (VP16), SN38 (the active metabolite of irinotecan) and taxol, are reported in Table I. The data reveal that bal6/7 displays higher anti-proliferative activity than etoposide and oxaliplatin, although the mixture was appreciably less active than SN38 and markedly less active than taxol. Bal6/7 demonstrated the highest activity against A549 NSCLC (IC_{50}, 0.3 μM) and U373 glioblastoma (IC_{50}, 0.5 μM) cell lines.

Bal6/7 effects on human A549 NSCLC and U373 glioblastoma cell morphology. Fig. 3A illustrates the typical morphology of untreated human A549 NSCLC cells at the beginning (t = 0 min) of image recording using computer-assisted phase-contrast microscopy, while Fig. 3B illustrates the situation 72 h later. Fig. 3C and D shows the corresponding still images at 0 min and 72 h of A549 NSCLC cells treated with bal6/7 at its IC_{75} of 470 nM (Table I). Fig. 3D shows that those A549 NSCLC cells that escaped the anti-proliferative/cytotoxic effects of bal6/7 displayed increased size and were more flattened in appearance than control A549 cells (Fig. 3A). These cells also moved more slowly indicative of a bal6/7 effect on cell migration. Such modifications of A549 cell shape on bal6/7 treatment are compatible with modifications to the actin cytoskeleton organization, a feature that has also been investigated in the present study. The video (data not shown) clearly indicates that bal6/7 did not induce detergent-like effects, as has been observed for some saponins, since no cell 'explosions' were observed. Fig. 3E-H illustrates the same effects of bal6/7 in human U373 glioblastoma cells as seen in A549 NSCLC cells.

Determination of potential bal6/7 effects on cell cycle progression and apoptosis in human A549 NSCLC and U373 glioblastoma cells. Fig. 4A shows that bal6/7 does not markedly modify A549 NSCLC or U373 glioblastoma cell

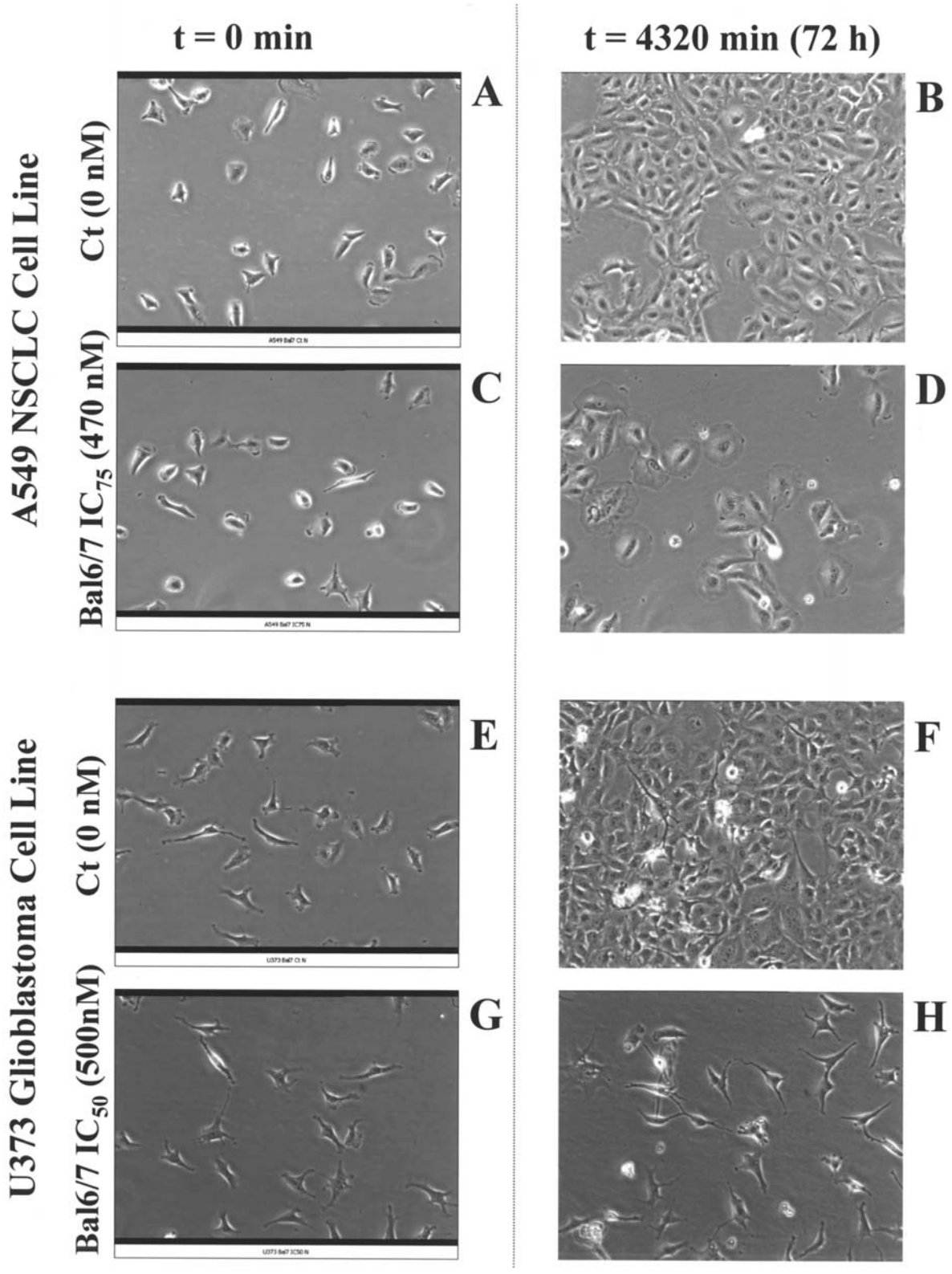

Figure 3. Bal 6/7 effects on cancer cell morphology and migration. Computer assisted videomicroscopy monitoring (real-time cellular imaging) of the effects of bal6/7 treatment on human A549 NSCLC and U373 glioblastoma cell proliferation and migration. The NSCLC A549 cells were either left untreated (A and B) or treated for 0-72 h with bal6/7 at the IC_{75} concentration of 470 nM (C and D). The glioblastoma U373 cells were either left untreated (E and F) or treated for 0-72 h with bal6/7 at the IC_{50} concentration of 500 nM (G and H). For paper versions, the last recorded still image for each experimental condition at 72 h is presented (B, D, F and H).

cycle kinetic parameters, i.e. the percentage of either of these cancer cells in the GO/G1, S and G2/M phases of the cell cycle, when treated with IC_{50} or IC_{75} concentrations of bal6/7 for up to 72h. In the same manner, bal6/7 at IC_{50} concentration induces neither early (annexin V-positive but PI-negative cells) nor late (annexin V-positive and PI-positive cells) apoptosis

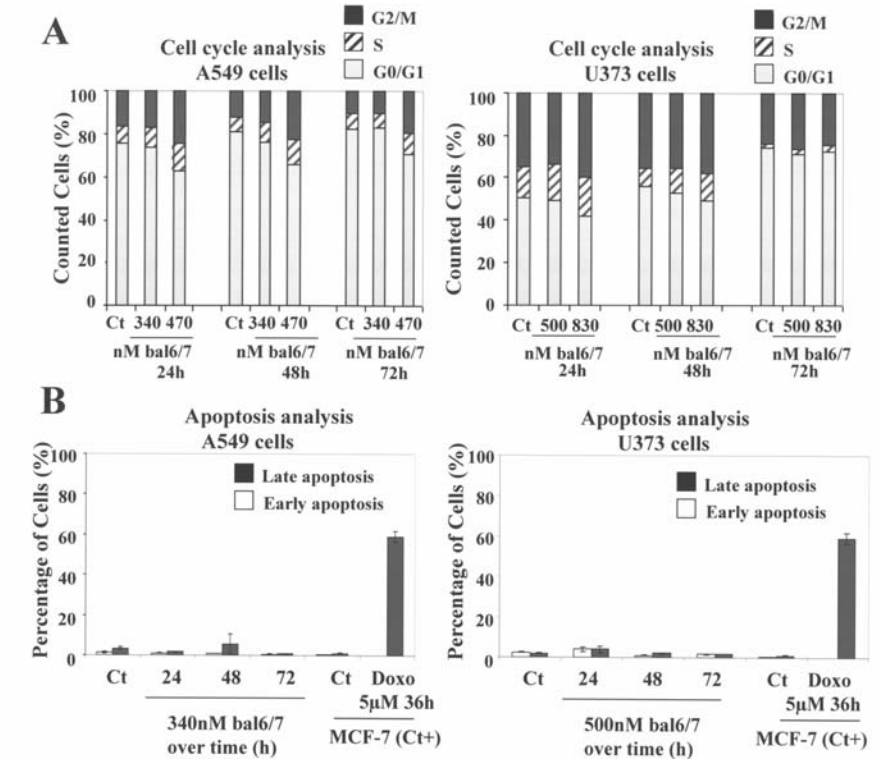

Figure 4. Effects of bal6/7 on the cell cycle and apoptosis in cancer cells. A, the effects of bal6/7 at IC_{50} and IC_{75} concentrations on the cell cycle kinetics of A549 and U373 cancer cells were assessed at 24, 48 and 72 h using flow cytometry. Each experiment was carried out in triplicate and panels illustrate the net results obtained. For the controls (Ct), cells were incubated with solvent alone. The areas shaded grey of each bar chart represent the proportion of cells in the G1 phase of their cell cycles, while the hatched and black areas represent the proportion of cells in the S and G2 phases, respectively. B, determination of the level of bal6/7-induced cell death monitored by flow cytometry over 24, 48 and 72 h in A549 NSCLC and U373 glioblastoma cells. The open bars represent the percentage of cells in early apoptosis while the black bars represent the proportion of cells in late apoptosis. MCF-7 human breast cancer cells incubated for 36 h in the presence of 5 μM doxorubicin were used as the positive control for the experiment. For the controls (Ct), cells were incubated with solvent alone. Each experiment was carried out in triplicate. The data are presented as the means ± their standard errors.

in either A549 NSCLC or U373 glioblastoma cells (Fig. 4B) unlike the positive control doxorubicin in MCF-7 breast cancer cells.

Characterization of bal6/7-induced effects on $[ATP]_i$ and $[ROS]_i$. Distinct classes of natural products exert their cytotoxic activity through depletion of $[ATP]_i$ which is accompanied (or induced) by an increase in $[ROS]_i$. While bal6/7 markedly decreased $[ATP]_i$ at its IC_{75} concentrations in A549 NSCLC (Fig. 5Aa) and U373 glioblastoma (Fig. 5Ab) cells, it did not modify $[ROS]_i$ (Fig. 5Ba and 5Bb) unlike the positive control used, H_2O_2 in MCF-7 breast cancer cells.

Reduction of bal6/7 cytotoxic effects by extraneous sugars or glycine. $[ATP]_i$ depletion could be the consequence of treatment-induced sustained glycolysis and/or proteolysis. Accordingly, $[ATP]_i$ could be maintained by extraneous sugars and/or glycine. The addition of D-glucose (Fig. 6A), L-fructose (Fig. 6B) or glycine (Fig. 6C) to A549 NSCLC and U373 GBM cell cultures 24 h prior to bal6/7 treatment, significantly ($p<0.05$ - <0.0001) reduced the cytotoxic effects of bal6/7, as revealed by the MTT colorimetric assay.

Bal6/7 markedly disorganizes the actin cytoskeleton. The observed marked impairment in A549 and U373 cell proliferation and migration, as well as ATP depletion following

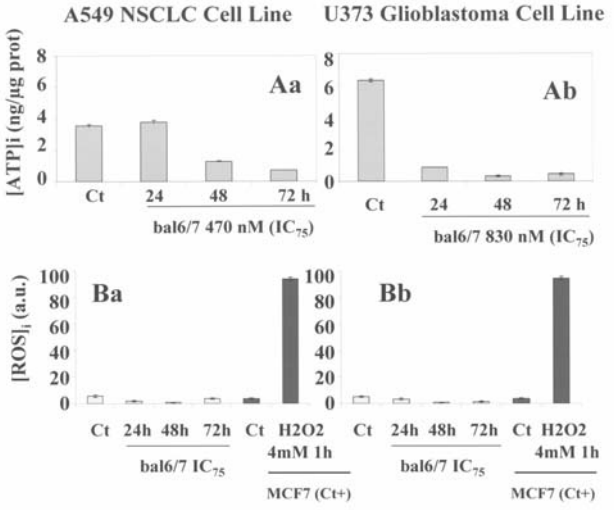

Figure 5. Effects of bal6/7 on $[ATP]_i$ and $[ROS]_i$ in cancer cells. A, determination of bal6/7-induced effects on $[ATP]_i$ in A549 NSCLC (Aa) and U373 glioblastoma (Ab) cells. Bal6/7 was evaluated for 24, 48 and 72 h at IC_{75} concentrations. Each determination was undertaken in triplicate and data are presented as the means ± their standard errors. For the controls (Ct), cells were incubated with the solvent alone. B, determination of bal6/7-induced effects on $[ROS]_i$ in A549 NSCLC (Ba) and U373 glioblastoma (Bb) cells. Bal6/7 was evaluated for 24, 48 and 72 h at IC_{75} concentrations. For the controls (Ct), cells were incubated with solvent alone. MCF-7 human breast cancer cells incubated for 1 h in the presence of 4 mM H_2O_2 were used as the positive control for the experiment. Each determination was undertaken in triplicate and is presented as the mean ± standard error.

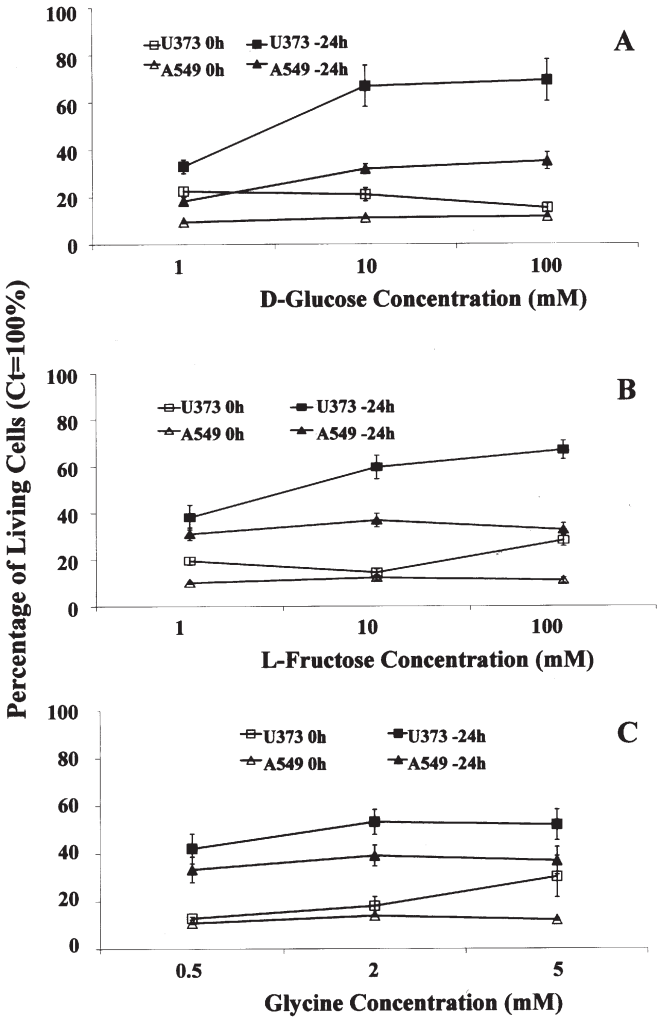

Figure 6. Reducing the cytotoxic effects of bal6/7. The effects of adding increasing concentrations of D-glucose (A: 1-100 mM), L-fructose (B: 1-100 mM) or glycine (C: 0.5-5 mM) to A549 NSCLC (triangles) and U373 GBM (squares) cultures, 24 h before (black symbols) or at the same time (open symbols) as bal6/7 treatment at IC_{50} concentrations, were investigated using the MTT colorimetric assay. Each evaluation was undertaken in sextuplicate and the data are presented as the means ± standard errors.

bal6/7 treatment, suggested that the mixture's effects might be mediated, at least partly, by the disorganization of the actin cytoskeleton. As shown in Fig. 7, bal6/7 indeed markedly and relatively rapidly over a 2-h period disorganized the actin cytoskeleton at its IC_{75} concentrations in A549 NSCLC as well as in U373 glioblastoma cells.

In vivo anti-tumor effects of bal6/7. The *in vivo* anti-tumor effects of bal6/7 were investigated in a primary screening model, the L1210 murine leukemia model (16) at three different dose levels: 5, 2.5 and 1.25 mg/kg i.p. corresponding to half of the maximal tolerated dose [MTD in mice: 10 mg/kg (data not shown), MTD/4 and MTD/8]. Bal6/7 weakly but significantly (p=0.01-0.03) increased the survival of mice bearing L1210 leukemia (Fig. 8) at all three evaluated doses. However, there was no evidence of a dose-related response. The potential therapeutic benefit contributed by bal6/7 was evaluated by means of the T/C index. According to the guidelines of the National Cancer Institute, USA, when a compound is associated with a T/C index value equal or superior to 125%, it is considered to be active. In this study, bal6/7 displayed a T/C index of 130% (at all tested dose levels) indicating that the mixture increased by 30% the survival time of mice bearing L1210 leukemia. The *in vivo* anti-tumor effects observed here with bal6/7 are of the same magnitude as those observed with vincristine in this model (16).

Discussion

Saponins to which balanitins belong are widely distributed in plants. Their surface-active properties are what distinguish these compounds from other glycosides. They readily dissolve in water to form colloidal solutions that foam upon shaking (20). Saponins have a broad range of biological properties. Most are haemolytic and are toxic to cold-blooded animals, while certain saponins also display molluscicidal, anti-inflammatory, anti-fungal/anti-yeast, anti-bacterial/anti-microbial, anti-parasitic and anti-viral activity. Numerous reports have also highlighted the highly cytotoxic properties of many saponins (reviewed in ref. 20). Saponins can act as potential anti-cancer agents by preventing carcinogenesis (21-23) or by exerting direct anti-proliferative and/or cytotoxic effects against cancer cells (24-28) even *in vivo* (26).

In the current study, it has been demonstrated that a mixture of balanitin-6 and balanitin-7 (referred to as bal6/7) displays anti-cancer activity both *in vitro* and *in vivo*. A cellular imaging-based approach (11-13,17) has also enabled demonstration that the anti-cancer activity of bal6/7 was not associated with membrane permeabilization or osmotic shock and thus did not appear to result from a detergent-like effect of the mixture (Fig. 3). The anti-tumor activity of bal6/7 results from the fact that it markedly decreases $[ATP]_i$ (without a discernible increase in intra-cellular ROS), and this decrease in $[ATP]_i$ induces in turn a marked disorganization of the actin cytoskeleton (17).

Distinct classes of natural products exert their cytotoxic activity through depletion of $[ATP]_i$. This is the case for example for cardiac glycosides (9,17), isocarbostyril alkaloids such as pancratistatin (29) and tetrandrine, a bisbenzyl tetrahydroisoquinoline alkaloid (30). Usually, a natural product-induced decrease in $[ATP]_i$ is accompanied by an increase in $[ROS]_i$ (29,30). This as indicated above is not the case for bal6/7 (Fig. 5). An $[ROS]_i$ increase is usually paralleled by activation of apoptosis (29,30) which once more was not the case with respect to bal6/7 (Fig. 4). In fact, the anti-tumor effects of bal6/7 seem to directly relate to a marked disorganization of the actin cytoskeleton (Fig. 7) through depletion of $[ATP]_i$ (Fig. 5). The bal6/7-mediated anti-tumor effects which seem to occur via $[ATP]_i$ depletion, are indeed significantly reduced when D-glucose, L-fructose or glycine is added 24 h prior to bal6/7 to the culture media of human U373 glioblastoma and A549 NSCLC cells (Fig. 6). Fructose (31) and glucose (32,33) protection is mediated by preservation of cellular ATP supply by glycolysis. Glycine cytoprotection against cellular ATP depletion occurs via a decrease in total cellular proteolysis (34). In other words, glycine could protect against cellular ATP depletion-induced cytotoxic effects by inhibiting proteolytic activities (34).

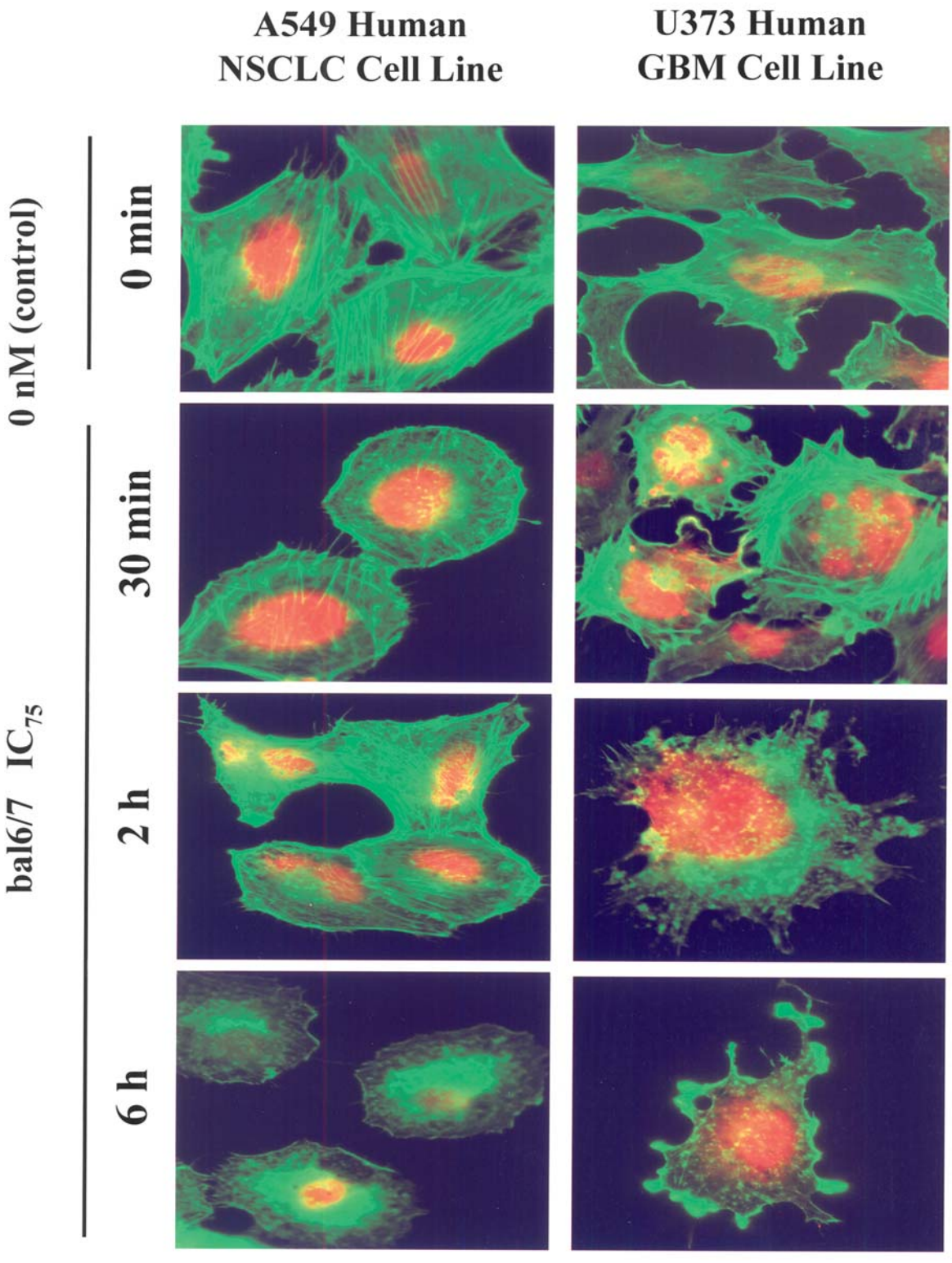

Figure 7. The effects of bal6/7 treatment on actin cytoskeleton organization. Actin distribution, fibrillar (green fluorescence) and globular (red fluorescence) forms in A549 NSCLC and U373 GBM cells, untreated (0 nM) and treated with bal6/7 for 0.5, 2 and 6 h at concentrations corresponding to their respective IC_{75} values.

The chemical hypoxia induced by bal6/7 in A549 NSCLC and U373 glioblastoma cells was not associated with mitochondrial membrane permeabilization (data not shown). In fact, measured ATP levels represent mainly the contribution of intact cells, as any ATP generated by functional mitochondria from highly permeable or completely disrupted cells would be rapidly hydrolyzed, much like exogenous ATP added to the incubation medium (35). As already emphasized, intracellular ATP depletion causes marked actin cytoskeletal disruption, as also evidenced in the current study (Fig. 7). In fact cellular ATP depletion in diverse cell types results in the net conversion of monomeric G-actin to polymeric F-actin. This conversion itself results from altering the ratio of ATP-G-actin and ADP-G-actin, causing a net decrease in the

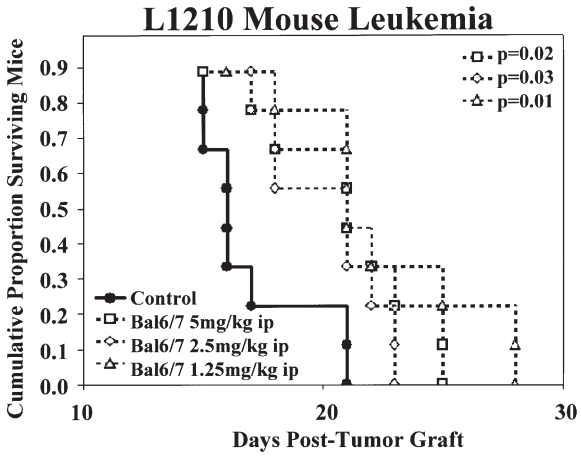

Figure 8. The *in vivo* anti-tumor effects of bal6/7 in the murine L1210 leukemia model. Bal6/7 was evaluated at dose levels of 5 mg/kg (open squares), 2.5 mg/kg (open diamonds), and 1.25 mg/kg (open triangles) administered i.p. 4 times a week for 2 consecutive weeks (days 1-4 and 8-11), with treatment starting the day following leukemia cell grafting to the mice (day 0). There were 9 mice per experimental group. The control mice (black circles) received the vehicle only. The presented plot displays the decreasing cumulative proportion of mice surviving in each group (Kaplan-Meier survival analysis).

concentration of thymosin-actin complexes as a consequence of the differential affinity of thymosin ß4 for ATP- and ADP-G-actin (36). Increased detection of profiling-actin complexes during depletion indicates that profiling may participate in catalyzing nucleotide exchange during depletion (36). Endothelial cell damage during simulated ischemia (reperfusion involves mitochondrial dysfunction, ATP depletion and ATP-dependent cytoskeletal disruption) is characterized by degradation of actin microfilaments, disappearance of focal adhesions and retraction of the cytoplasm (33). In other cell types, including mouse embryo fibroblasts (37), mouse leukemia cells (38), microvilli of the apical membrane of proximal tubule cells (39) and human NSCLC cells (17), ATP depletion also causes major perturbation of the actin cytoskeleton's organization. A functional actin cytoskeleton is vital for cell proliferation (during cytokinesis for example) and migration (40). Thus, it seems likely that the anti-tumor effects associated with bal6/7 can be explained at least partly, by the bal6/7-induced depletion in $[ATP]_i$ which results in a major disorganization of the actin cytoskeleton.

The *in vivo* anti-tumor effects obtained with bal6/7, although modest, are nevertheless statistically significant. These preliminary *in vivo* data give some hope of developing more selective and potent balanitin derivatives for combating cancer. Balanitin-6 and -7, like dioscin and polyphyllin D, belong to a group of structurally similar diosgenyl saponins which can be synthesized by stepwise glycosylation (7). It should therefore be possible to generate novel hemi-synthetic derivatives of balanitin-6 and -7 with potentially improved *in vitro* and *in vivo* anti-cancer activity and reduced *in vivo* toxicity, and thus a markedly improved therapeutic ratio. This approach has already been successfully applied to certain types of cardenolides (9) and marine pyridoacridines [ascididemin and meridine (41)] and quinolone derivatives (42). Also, it has already been demonstrated that saponins from *Tribulus terrestris* L are less toxic to normal human fibroblasts than many cancer cell lines (28), giving further hope of synthesizing balanitins with improved therapeutic ratios.

In playing a major role in mitosis, cell signaling and migration, microtubules and actin filaments are potentially interesting anti-cancer targets (43,44). However, while several anti-tubulin drugs (of natural origin) are already marketed for cancer (Paclitaxel®, Taxotere®, Navelbine®, Oncovin®, etc), no anti-actin compounds are yet marketed as anti-cancer drugs (13,17). The actin cytoskeleton represents a target against which a number of academic and pharmaceutical organizations are attempting to develop selective inhibitors to fight cancer (13,17,43-47). Thus, novel derivatives of balanitins could have high therapeutic potential in cancer.

In conclusion, bal6/7-mediated *in vitro* non-apoptotic anti-cancer activities rely on depletion of $[ATP]_i$ leading to major disorganization of the actin cytoskeleton. The modest but nevertheless statistically significant *in vivo* activity of bal6/7 increases the possibility of developing more selective anti-cancer balanitin derivatives.

Acknowledgments

We would like to acknowledge the scientific contribution and advice of Dr V. Facchini in the finalisation of this article. The present study was supported by grants provided by the Fonds Yvonne Boël (Brussels, Belgium). C. Gnoula is a grant holder from the Université Libre de Bruxelles. R. Kiss is a Director of Research with the Fonds National de la Recherche Scientifique (FNRS, Belgium) and F. Lefranc is a Clinical Research Fellow with the FNRS.

References

1. Kamel MS and Koskinen A: Pregnane glycosides from fruits of Balanites aegyptiaca. Phytochemistry 40: 1773-1775, 1995.
2. Speroni E, Cervellati R, Innocenti G, Costa S, Guerra MC, Dall'Acqua S and Govoni P: Anti-inflammatory, anti-nociceptive and antioxidant activities of Balanites aegyptiaca (L.) Delile. J Ethnopharmacol 98: 117-125, 2005.
3. Koko WS, Galal M and Khalid HS: Fasciolicidal efficacy of Albizia anthelmintica and Balanites aegyptiaca compared with albendazole. J Ethnopharmacol 71: 247-252, 2000.
4. Kamel MS: A furostanol saponin from fruits of Balanites aegyptiaca. Phytochemistry 48: 755-757, 1998.
5. Sarker SD, Bartholomew B and Nash RJ: Alkaloids from Balanites aegyptiaca. Fitoterapia 71: 328-330, 2000.
6. Koko WS, Abdalla HS, Galal M and Khalid HS: Evaluation of oral therapy on Mansonial Shistosomiasis using single dose of Balanites aygyptiaca fruits and praziquantel. Fitoterapia 76: 30-34, 2005.
7. Deng S, Yu B, Hui Y, Yu H and Han X: Synthesis of three diosgenyl saponins: dioscin, polyphyllin D and balanitin-7. Carbohydrate Res 317: 53-62, 1999.
8. Pettit GR, Doubek DL, Herald DL, Numata A, Takahasi C, Fujiki R and Miyamoto T: Isolation and structure of cytostatic steroidal saponins from the African medicinal plant Balanites aegyptiaca. J Nat Prod 54: 1491-1502, 1991.
9. Van Quaquebeke E, Simon G, Andre A, *et al*: Identification of a novel cardenolide (2"-oxovorusharin) from Calotropis procera and the hemisynthesis of novel derivatives displaying potent *in vitro* antitumor activities and high *in vivo* tolerance: Structure-activity relationship analyses. J Med Chem 48: 849-856, 2005.
10. Ingrassia L, Nshimyumukiza P, Dewelle J, *et al*: A lactosylated steroid contributes *in vivo* therapeutic benefits in experimental models of mouse lymphoma and human glioblastoma. J Med Chem 49: 1800-1807, 2006.
11. Debeir O, Van Ham P, Kiss R and Decaestecker C: Tracking of migrating cells under phase-contrast video microscopy with combined mean-shift processes. IEEE Trans Med Imaging 24: 697-711, 2005.

12. Decaestecker C, Debeir O, Van Ham P and Kiss R: Can anti-migratory drugs be screened *in vitro*? A review of 2D and 3D assays for the quantitative analysis of cell migration (Review). Med Res Rev 27: 149-176, 2007.
13. Hayot C, Debeir O, Van Ham P, Van Damme M, Kiss R and Decaestecker C: Characterization of the activities of actin-affecting drugs on tumor cell migration. Toxicol Appl Pharmacol 211: 30-40, 2006.
14. Mathieu A, Remmelink M, D'Haene N, *et al*: Development of a chemoresistant orthotopic human non small cell lung carcinoma model in nude mice: analyses of tumor heterogenity in relation to the immunohistochemical levels of expression of cyclo-oxygenase-2, ornithine decarboxylase, lung-related resistance protein, prostaglandin E synthetase, and glutathione-S-transferase-alpha (GST)-alpha, GST-mu, and GST-pi. Cancer 101: 1908-1918, 2004.
15. Lefranc F, James S, Camby I, *et al*: Combined cimetidine and temozolomide, compared with temozolomide alone: significant increases in survival in nude mice bearing U373 human glioblastoma multiforme orthotopic xenografts. J Neurosurg 102: 706-714, 2005.
16. Darro F, Decaestecker C, Gaussin JF, Mortier S, Van Ginckel R and Kiss R: Are syngeneic mouse tumor models still valuable experimental models in the field of anti-cancer drug discovery? Int J Oncol 27: 607-616, 2005.
17. Mijatovic T, Roland I, Van Quaquebeke E, *et al*: The α1 subunit of the sodium pump could represent a novel target to combat non-small cell lung cancers. J Pathol 212: 170-179, 2007.
18. de Launoit Y, Veilleux R, Dufour M, Simard J and Labrie F: Characteristics of the biphasic action of androgens and of the potent antiproliferative effects of the new pure antiestrogen EM-139 on cell cycle kinetic parameters in LNCaP human prostatic cancer cells. Cancer Res 51: 5165-5170, 1991.
19. Darzynkiewicz Z, Juan G, Li X, Gorczyca W, Murakami T and Traganos F: Cytometry in cell neurobiology: Analysis of apoptosis and accidental cell death (necrosis). Cytometry 27: 1-20, 1997.
20. Sparg SG, Light ME and van Staden J: Biological activities and distribution of plant saponins. J Ethnopharmacol 94: 219-243, 2004.
21. Rao AV and Sung MK: Saponins as anticarcinogens. J Nutr 125: 717S-724S, 1995.
22. Konoshima T: Anti-tumor-promoting activities of triterpenoid glycosides; cancer chemoprevention by saponins. Adv Exp Med Biol 404: 87-100, 1996.
23. Kerwin SM: Soy saponins and the anticancer effects of soybeans and soy-based foods. Curr Med Chem Anticancer Agents 4: 263-272, 2004.
24. Drissi A, Bennani H, Giton F, Charrouf Z, Fiet J and Adlouni A: Tocopherols and saponins derived from Argania spinosa exert an antiproliferative effect on human prostate cancer. Cancer Invest 24: 588-592, 2006.
25. Gao J, Huang F, Zhang J, Zhu G, Yang M and Xiao P: Cytotoxic cycloartane triterpene saponins from Actaea asiatica. J Nat Prod 69: 1500-1502, 2006.
26. Tin MM, Cho CH, Chan K, James AE and Ko JK: Astragalus saponins induce growth inhibition and apoptosis in human colon cancer cells and tumor xenograft. Carcinogenesis 28: 1347-1355, 2007.
27. Ma YX, Fu HZ, Li M, Sun W, Xu B and Cui JR: An anticancer effect of a new saponin component from Gymnocladus chinensis Baillon through inactivation of nuclear factor-kappa B. Anticancer Drugs 18: 41-46, 2007.
28. Neychev VK, Nikolova E, Zhelev N and Mitev VI: Saponins from Tribulus terrestris L are less toxic for normal human fibroblasts than for many cancer lines: influence of apoptosis and proliferation. Exp Biol Med 232: 126-133, 2007.
29. Kekre N, Griffin C, McNulty J and Pandey S: Pancratistatin causes early activation of caspase-3 and the flipping of phosphatidyl serine followed by rapid apoptosis specifically in human lymphoma cells. Cancer Chemother Pharmacol 56: 29-38, 2005.
30. Yan C, Xin-Ming Q, Li-Kun G, *et al*: Tetrandrine-induced apoptosis in rat primary hepatocytes is initiated from mitochondria: caspases and endonuclease G (Endo G) pathway. Toxicology 218: 1-12, 2006.
31. Nieminen AL, Saylor AK, Herman B and Lemasters JJ: ATP depletion rather than mitochondrial depolarization mediates hepatocyte killing after metabolic inhibition. Am J Physiol Cell Physiol 36: C67-C74, 1994.
32. Nishimura Y, Romer LH and Lemasters JJ: Mitochondrial dysfunction and cytoskeletal disruption during chemical hypoxia to cultured rat hepatic sinusoidal endothelial cells: the pH paradox and cytoprotection by glucose, acidotic pH, and glycine. Hepatology 27: 1039-1049, 1998.
33. Terry C, Dhawan A, Mitry RR, Lehec SC and Hughes RD: Preincubation of rat and human hepatocytes with cytoprotectants prior to cryopreservation can improve viability and function upon thawing. Liver Transpl 12: 165-177, 2006.
34. Dickson RC, Bronk SF and Gores GJ: Glycine cytoprotection during lethal hepatocellular injury from adenosine triphosphate depletion. Gastroenterology 102: 2098-2107, 1992.
35. Weinberg JM, Davis JA, Abarzva M and Rajan T: Cytoprotective effects of glycine and glutathione against hypoxic injury to renal tubules. J Clin Invest 80: 1446-1454, 1987.
36. Atkinson SJ, Hosford MA and Molitoris BA: Mechanism of actin polymerization in cellular ATP depletion. J Biol Chem 279: 5194-5199, 2004.
37. Bershadsky AD, Gelfand VI, Svitkina TM and Tint IS: Destruction of microfilament bundles in mouse embryo fibroblasts treated with inhibitors of energy metabolism. Exp Cell Res 127: 421-429, 1980.
38. Hinshaw DB, Armstrong BC, Burger JM, Beals TF and Hyslop PA: ATP and microfilaments in cellular oxidant injury. Am J Pathol 132: 479-488, 1988.
39. White P, Gu L and Chen J: Decreased actin solubility observed during ATP-depletion is mimicked by severing agents but not depolymerizing agents in isolated and cultured proximal tubular cells. Clin Physiol Funct Imaging 22: 312-319, 2002.
40. Ono S: Mechanism of depolymerization and severing of actin filaments and its significance in cytoskeletal dynamics. Int Rev Cytol 258: 1-82, 2007.
41. Delfourne E, Kiss R, Le Corre L, *et al*: Synthesis and *in vitro* antitumor activity of phenanthrolin-7-one derivatives, analogues of the marine pyridoacridine alkaloids ascididemin and meridine: structure-activity relationship. J Med Chem 46: 3536-3545, 2003.
42. Joseph B, Darro F, Behard A, *et al*: 3-Aryl-2-quinolone derivatives: synthesis and characterization of *in vitro* and *in vivo* antitumor effects with emphasis on a new therapeutical target connected with cell migration. J Med Chem 45: 2543-2555, 2002.
43. Jordan MA and Wilson L: Microtubules and actin filaments: dynamic targets for cancer chemotherapy. Curr Opin Cell Biol: 10: 123-130, 1998.
44. Fenteany G and Zhu S: Small-molecule inhibitors of actin dynamics and cell motility. Curr Top Med Chem 3: 593-616, 2003.
45. Giganti A and Friederich E: The actin cytoskeleton as a therapeutic target: state of the art and future directions. Prog Cell Cycle Res 5: 511-525, 2003.
46. Fritz G and Kaina B: Rho GTPases: promising cellular targets for novel anticancer drugs. Curr Cancer Drug Targets 6: 1-14, 2006.
47. Stehn JR, Schevzov G, O'Neill GM and Gunning PW: Specialisation of the tropomyosin composition of the actin filaments provides new potential targets for chemotherapy. Curr Cancer Drug Targets 6: 245-256, 2006.